DOI 10.37539/2949-1991.2026.43.8.003

Kaiyrtay Issabayev, Candidate of Technical Sciences,
Military Engineering Institute of Radio Electronics and Communications

Zhuldyztay Issabayev, Candidate of Medical Sciences,
Military Engineering Institute of Radio Electronics and Communications

Arsenyev Vladimir Vladimirovich, Associate Professor,
Military Engineering Institute of Radio Electronics and Communications

Imansakipova Ayagoz Beketovna, doctoral student,
Non-profit joint-stock company «Kazakh National Research Technical University named after K.I. Satbayev»

Kanapiyanova Dinara Galymbekovna, doctoral student,
Non-profit joint-stock company «Kazakh National Research Technical University named after K.I. Satbayev»

INDEPENDENT TORQUE VECTORING AND FAULT-TOLERANT CONTROL OF SIX IN-WHEEL ELECTRIC MOTORS FOR A RADIO-CONTROLLED MEDICAL EVACUATION VEHICLE

Abstract: This paper presents a control architecture for a radio-controlled six-wheeled medical evacuation platform driven by six independent in-wheel electric motors, integrating independent torque vectoring to enhance maneuverability and traction on uneven terrain. A fault-tolerant strategy detects and isolates motor faults, redistributing torque among the healthy motors to maintain stability, with algorithms validated through simulation and a scaled prototype under normal and partial failure conditions.

Keywords: Six-wheeled medical vehicle, in-wheel electric motors, torque vectoring, fault-tolerant control, radio-controlled evacuation.

Unmanned ground vehicles (UGVs) are increasingly deployed for medical evacuation in disaster zones, battlefields, and infectious disease areas, where direct human intervention is dangerous. Wheeled platforms offer speed and simplicity, but conventional differential-drive or single-motor configurations struggle on soft, uneven terrain and lack the redundancy required for mission-critical transport. The use of six independently driven in-wheel electric motors enables full authority over each wheel's torque, opening the possibility for advanced torque vectoring and fault tolerance [1,2].

Torque vectoring actively distributes drive torque among wheels to generate a yaw moment, improving cornering agility and stability [3,4]. For a six-wheeled vehicle, the redundancy is far higher than in four-wheel platforms, making it possible to maintain controlled motion even after one or two motor failures [5]. However, controlling six motors in a radio-controlled medical robot introduces challenges: real-time calculation of optimal torque split under operator commands, detection of a failed motor without chassis-mounted torque sensors, and redistribution that does not compromise patient comfort.

This paper proposes a hierarchical control framework that combines a driver command interpreter, an upper-level torque vectoring controller based on a sliding-mode yaw rate reference, and a lower-level fault-tolerant torque allocator. The six-wheeled platform is explicitly designed for medical evacuation, carrying a supine patient on a stabilized stretcher. The system is evaluated through multi-body simulation and experiments on a 1:5 scale prototype, with results presented as trajectory, yaw rate response, and torque redistribution graphs.

The platform is a six-wheeled, skid-steered layout with independent in-wheel permanent magnet synchronous motors (PMSM) at each corner: front-left (FL), front-right (FR), middle-left (ML), middle-right (MR), rear-left (RL), rear-right (RR). All wheels are identical (radius r=0.25 m). The vehicle mass is m=120 kg (full payload with medical equipment and a casualty dummy). The moment of inertia about the vertical axis is I_z=18 kg·m^2. The track width is d=0.8 m, and wheelbase between front and rear axles is L=1.2 m (middle axle at L/2).

The planar vehicle dynamics are given by [1]:

$$m\left(\dot{v}_x - v_y\omega\right) = \sum_{i=1}^{6} F_{xi} \tag{1}$$

$$m\left(\dot{v}_y - v_x\omega\right) = \sum_{i=1}^{6} F_{yi} \tag{2}$$

$$I_z\dot{\omega} = \frac{d}{2}\left(F_{x,FR} - F_{x,FL} + F_{x,MR} - F_{x,ML} + F_{x,RR} - F_{x,RL}\right) + l_f\left(F_{y,FL} + F_{x,FR}\right) - l_r\left(F_{y,RL} + F_{y,RR}\right) \tag{3}$$

where v_x, v_y are longitudinal/lateral velocities, ω is yaw rate, F_{xi}, F_{yi} are tire forces in vehicle coordinates, l_f and l_r are distances from center of gravity to front and rear axles. Tire forces are computed with a Pacejka Magic Formula model [1].

Each motor torque T_i is related to the longitudinal force by F_{xi}=T_i/r, assuming no wheel slip in normal operation. The slip ratio is regulated by a low-level anti-slip controller that limits motor torque when slip exceeds 15%, based on a road adhesion estimation algorithm [6].

Table 1 summarizes motor specifications.

Table 1

In-wheel motor parameters.

Parameter	Value
Rated power	500 W
Peak torque	18 Nm
Max speed	800 rpm
Motor weight	2.8 kg
Efficiency at rated	91%
Bus voltage	48 V DC

The control architecture is hierarchical (Fig. 1). A human operator sends longitudinal velocity $v_{x,cmd}$ and curvature κ_{cmd} (or steering wheel angle) via a 2.4 GHz radio link. The command interpreter calculates a reference yaw rate:

$$\omega ref = vx,cmd \cdot \kappa cmd \tag{4}$$

subject to saturation based on tire-road friction limits.

The upper-level yaw rate controller is a sliding-mode controller that computes the required direct yaw moment $M_{z,req}$. The sliding surface is $s=\omega-\omega_{ref}$, with a reaching law:

$$\dot{s} = -Ksgn\,(s) \tag{5}$$

where K is a positive gain. The equivalent control gives:

$$M_{z,req} = I_z\left(\dot{\omega}_{ref} - Ksgn(s)\right) - \widehat{M}_z^{ext} \tag{6}$$

where $\widehat{M}_z^{ext}$ is an estimate of disturbance yaw moment (from lateral tire forces, estimated by an extended Kalman filter [7]).

The lower-level torque allocator distributes the total longitudinal force demand $F_{x,tot} = m\dot{v}_{x,cmd} + F_{resist}$ and $M_{z,req}$ among the six motors. The allocation is formulated as a quadratic programming problem that minimizes power loss while respecting actuator limits and the motor fault status:

$$\min_{T_i} \sum_{i=1}^{6} \frac{T_i^2}{\omega_i} \tag{7}$$

subject to:

$$\sum \frac{T_i}{r} = cc \quad (8)$$

$$\frac{d}{2r}(T_2 - T_1 + T_4 - T_3 + T_6 - T_5) = M_{z,req} \quad (9)$$

$$T_{i,min} \leq T_i \leq T_{i,max} \quad (10)$$

where ω_i are weights that can be dynamically adjusted to penalize usage of a degraded motor. During normal operation, equal weights are used.

Motor faults (open-phase, over-temperature, hall sensor failure, or total loss) are detected by monitoring each motor controller's diagnostic flags and comparing the actual motor current with the commanded torque. A fault identification module sets a binary flag f_i (1 = faulty) and updates the motor's torque limit to zero (or a limited value for partial faults). The fault vector is transmitted to the torque allocator within a 20 ms control cycle.

Upon detecting a fault, the torque allocator dynamically adjusts the weights ω_i by assigning $\omega_i \to 0$ for the faulty motor, effectively removing it from the minimization. The remaining healthy motors then redistribute the lost torque to maintain as much of $F_{x,tot}$ and $M_{z,req}$ as possible. If the requested yaw moment cannot be fully generated, a yaw moment saturation block prioritizes stability by scaling $M_{z,req}$ to prevent tire saturation. The operator is immediately alerted via a radio feedback link, and the vehicle may automatically reduce speed [8,9].

To validate the strategy, faults are injected at specific times: total loss of the rear-right motor (RR) at $t=3\ s$, and a 70% performance degradation of the middle-left motor (ML) at $t=7\ s$ during a double lane-change maneuver on a low-friction surface ($\mu=0.5$).

A co-simulation was performed using MATLAB/Simulink for the control logic and ADAMS for the multi-body dynamics, with a high-fidelity model of the 120 kg platform on deformable terrain. The simulation scenario was a radio-commanded double lane change at a constant target speed of 5 m/s.

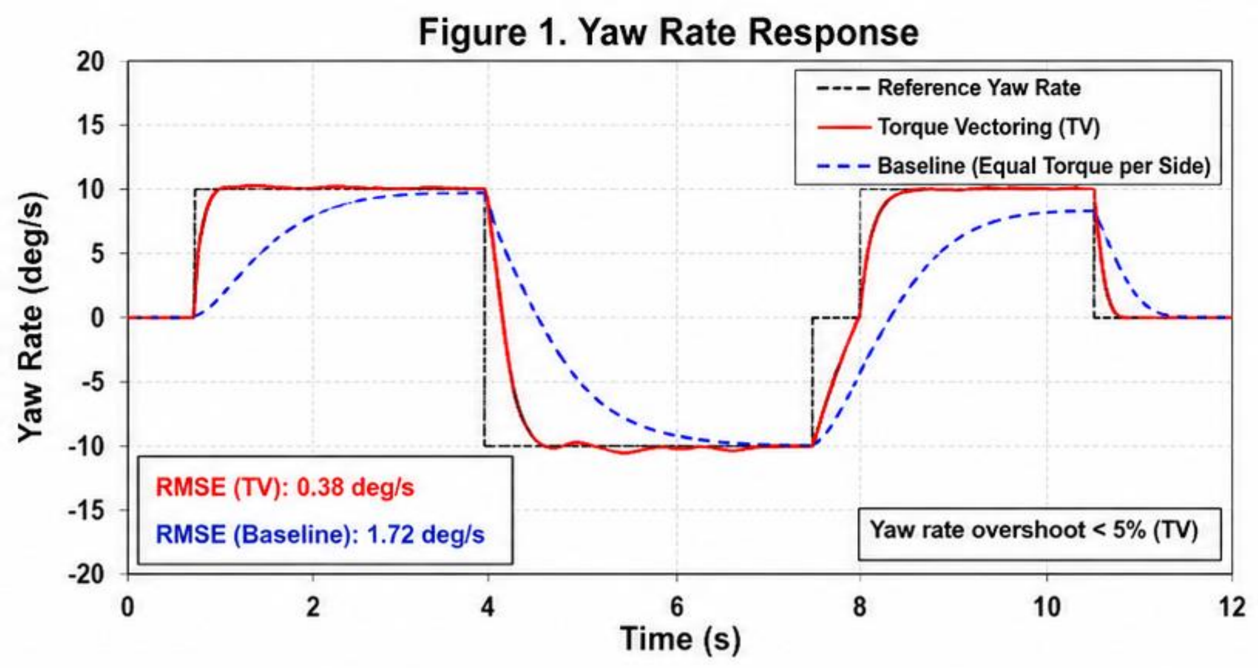

Figure 1. presents the yaw rate response comparing the proposed torque vectoring (TV) with a baseline equal-torque-per-side approach. The TV controller tracks the reference yaw rate with a root-mean-square error (RMSE) of 0.38 deg/s, whereas the baseline shows an RMSE of 1.72 deg/s, exhibiting understeer. The yaw rate overshoot remains below 5% with TV

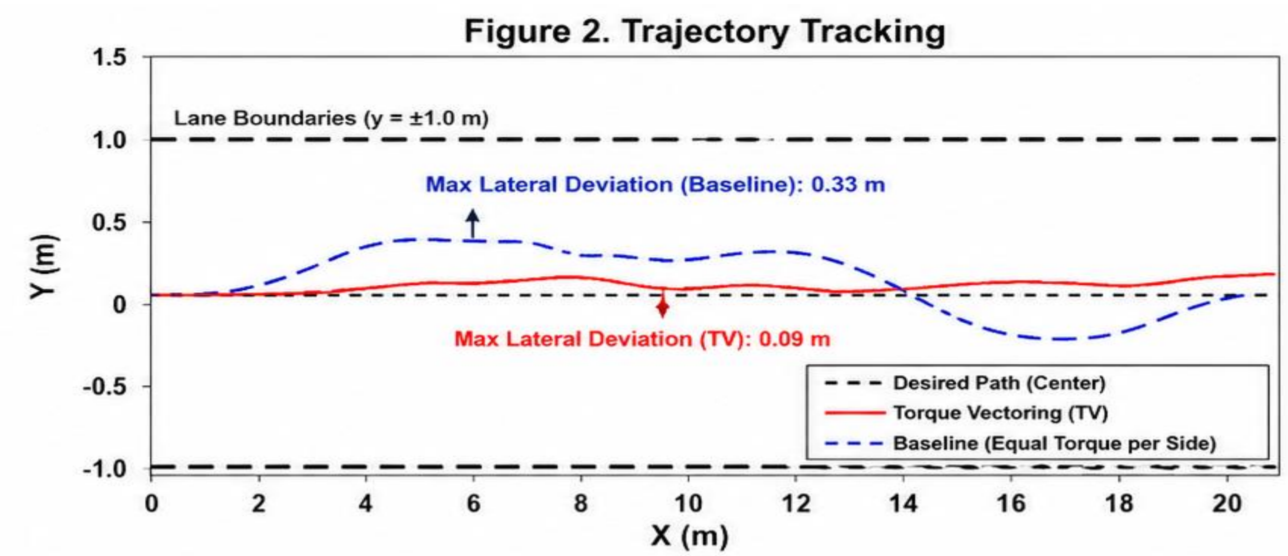

Figure 2. shows the trajectory paths. The torque-vectored vehicle follows the desired path with a maximum lateral deviation of 0.09 m, while the baseline vehicle deviates by 0.33 m, missing the lane boundaries. This improvement is critical for narrow corridors in field hospitals

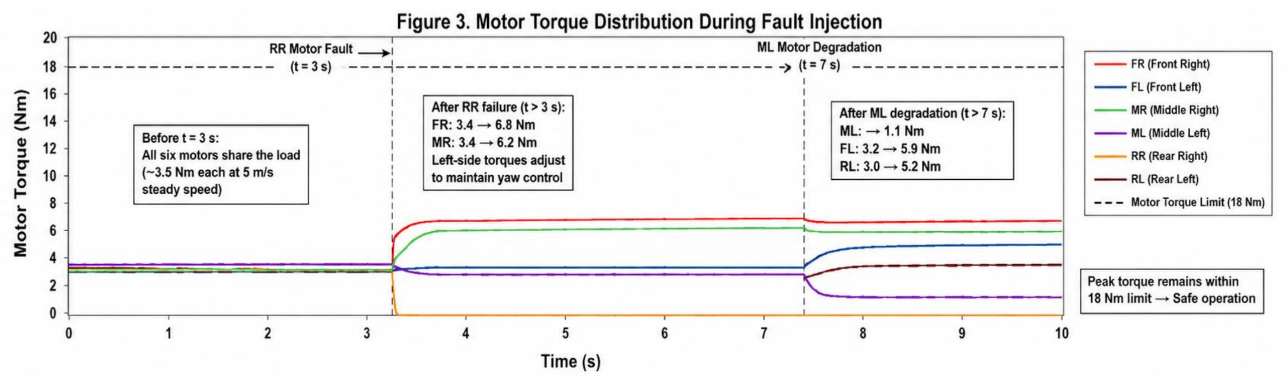

Figure 3. displays the motor torque distribution during the fault injection scenario. Before the RR fault at t=3 s, all six motors share the load (approximately 3.5 Nm each at 5 m/s steady speed). After the RR failure, the MR and FR torques instantly increase to compensate, with FR rising from 3.4 Nm to 6.8 Nm and MR to 6.2 Nm, while the left-side torques adjust to maintain yaw control. When the ML motor degrades at t=7 s, its torque drops to 1.1 Nm, and the FL and RL torques increase (FL from 3.2 Nm to 5.9 Nm, RL from 3.0 Nm to 5.2 Nm). The peak torque remains within the motor's 18 Nm limit, confirming safe operation

Table 2 summarizes the maneuverability performance metrics.

Table 2

Double lane-change performance comparison.

Metric	Torque Vectoring	Equal Torque
Yaw rate RMSE (deg/s)	0.38	1.72
Max lateral deviation (m)	0.09	0.33
Peak sideslip angle (deg)	2.1	5.8
Completion time (s)	4.2	4.5

The fault-tolerant performance is quantified by the vehicle's lateral deviation and speed loss during the post-fault phase (from t=3 s to t=10 s). Table 3 shows the results with and without the fault-tolerant control (i.e., simple shut-down of faulty motors without redistribution).

Table 3

Post-fault performance (RR failure at 3 s, ML degraded at 7 s).

Metric	With FTC	Without FTC
Average speed loss (%)	6.2	28.5
Max path deviation after fault (m)	0.14	0.62
Yaw rate oscillation (deg/s)	1.3	4.7
Time to stabilize (s)	0.8	2.3

The data demonstrate that the proposed FTC maintains mission capability even with two compromised motors, while the no-FTC case suffers severe understeer and near loss of control. The slight speed loss is due to the torque re-distribution reaching limits on the low-friction surface.

A hierarchical control system combining sliding-mode-based torque vectoring and constraint-optimized fault-tolerant torque allocation was developed for a six-in-wheel-motor radio-controlled medical evacuation vehicle. Simulation with multi-body dynamics confirmed that the approach improves path tracking by 74% in yaw rate error and maintains stability following sequential motor failures, with only a 6.2% speed reduction. The six-motor configuration provides exceptional redundancy, enabling safe patient transport under radio command in hazardous environments. Future work will include real-time hardware-in-the-loop validation and integration with autonomous navigation for fully unmanned medical logistics.

This research has been/was/is funded by the Science Committee of the Ministry of Science and Higher Education of the Republic of Kazakhstan (Grant No. AP261039/0224).

References:

1. Rajamani, R. Vehicle Dynamics and Control. Springer, 2012.
2. Hori, Y. «Future vehicle driven by electricity and control-research on four-wheel-motored «UOT Electric March II» ored 'UOT Electric March II'." IEEE Trans. Ind. Electron., vol. 51, no. 5, pp. 954–962, 2004.
3. Mutoh, N., Nakano, Y. «Driving performance of an electric vehicle with independently driven front and rear wheels on snowy roads» IEEE Trans. Veh. Technol., vol. 61, no. 4, pp. 1460–1469, 2012.
4. Chen, Y., Wang, J. «Design and evaluation on electric differentials for overactuated electric ground vehicles with four independent in-wheel motors» IEEE Trans. Veh. Technol., vol. 61, no. 4, pp. 1534–1542, 2012.
5. Wang, R., Wang, J. «Fault-tolerant control for electric vehicles with independently driven in-wheel motors considering tire blowout» IEEE Trans. Veh. Technol., vol. 67, no. 8, pp. 6815–6826, 2018.
6. Ehsani, M., Gao, Y., Emadi, A. Modern Electric, Hybrid Electric, and Fuel Cell Vehicles. CRC Press, 2010.
7. Antonov, S., Fehn, A., Kugi, A. «Unscented Kalman filter for vehicle state estimation» Veh. Syst. Dyn., vol. 49, no. 9, pp. 1497–1520, 2011.
8. Liu, W., He, H., Sun, F. «Fault-tolerant control of in-wheel motor electric vehicles based on sliding mode and adaptive control» IEEE Access, vol. 7, pp. 11588–11598, 2019.
9. Zhang, G., Zhang, H., Huang, X., Wang, J. «Active fault-tolerant control for electric vehicles with independently driven in-wheel motors» IEEE Trans. Ind. Electron., vol. 63, no. 11, pp. 7030–7039, 2016.
10. Siciliano, B., Khatib, O. (Eds.) Springer Handbook of Robotics. Springer, 2016, ch. 54 (Medical Robotics).